Experimental Evolution of Cell Shape in Bacteria

P.R.J. Yulo⌘[1], N. Desprat⌘[2,3], M.L. Gerth[4], Y. Liu[1], X.X. Zhang[1], P.B. Rainey[5,6,7] & H.L. Hendrickson[1,¥]

[1] *Institute of Natural and Mathematical Science, Massey University, Auckland.*
[2] *Laboratoire de Physique Statistique, Ecole Normale Supérieure, PSL Research University; Université Paris Diderot Sorbonne Paris-Cité; Sorbonne Universités UPMC Univeristés Paris 06; CNRS; 24 rue Lhomond, 75005 Paris, France.*
[3] *Paris Diderot University, 10 rue Alice Domon et Leonie Duquet. 75013 Paris, France.*
[4] *School of Biological Sciences, Victoria University of Wellington, PO Box 600, 6140, Wellington, New Zealand.*
[5] *New Zealand Institute for Advanced Study, Massey University, 0745, Auckland, New Zealand*
[6] *Department of Microbial Population Biology, Max Planck Institute for Evolutionary Biology, Plön, Germany.*
[7] *Laboratoire de Génétique de l'Evolution, Ecole Superieure de Physique et de Chimie Industrielles de la Ville de Paris (ESPCI Paris Tech), CNRS UMR 8231, PSL Research University, 75231 Paris, France.*

⌘These authors contributed equally to this work.

¥ Corresponding author, H.Hendrickson@massey.ac.nz

Cell shape is a fundamental property in bacterial kingdom. MreB is a protein that determines rod-like shape, and its deletion is generally lethal. Here, we deleted the *mreB* homolog from rod-shaped bacterium *Pseudomonas fluorescens* SBW25 and found that *ΔmreB* cells are viable, spherical cells with a 20% reduction in competitive fitness and high variability in cell size. We show that cell death, correlated with increased levels of elongation asymmetry between sister cells, accounts for the large fitness reduction. After a thousand generations in rich media, the fitness of evolved *ΔmreB* lines was restored to ancestral levels and cells regained symmetry and ancestral size, while maintaining spherical shape. Using population sequencing, we identified pbp1A, coding for a protein involved in cell wall synthesis, as the primary target for compensatory mutations of the *ΔmreB* genotype. Our findings suggest that reducing elongasome associated PBPs aids in the production of symmetric cells when MreB is absent.

Keywords: Cell shape, Evolution, Experimental Evolution, Coccoid, MreB, Pbp1A, OprD, Single cell analysis, Cell wall synthesis, Asymmetry.

1 Introduction

Bacterial cell shape is the result of the coordinated action of a suite of enzymes involved in cell wall construction, DNA segregation and cell division[1-6]. These are highly interdependent processes that can be difficult to genetically disentangle[7]. Cell shape is far from fixed on evolutionary time scales and is a key trait mediating bacterial fitness and adaptation[1]. Rod-like shape is hypothesized to be ancestral in bacteria but a myriad of shapes have successfully developed[5,8-10]. One of the key determinants of rod-like cell shape is MreB, the prokaryotic structural homolog of actin[11,12]. MreB is the molecular linchpin of rod-like shape and its loss is hypothesized to be either a primary or very early event in the transition between rod-like and spherical cell shape in bacteria[5,8-10,13-17].

MreB acts as a dynamic platform that directs the timing and location of a complex of cell wall elongation enzymes, the 'elongasome'[18] including the bi-functional lateral cell wall synthesis enzyme, Pencillin Binding Protein 1a (PBP1a)[19]. PBP1a and the other members of the elongasome complex move along the inner membrane of rod-like cells, manufacturing the growing peptidoglycan cell wall[20-23,24]. There is also growing evidence that MreB actively straightens cells during growth by associating with and directing the elongasome to regions of negative curvature in cell walls[25,26]. In addition, MreB disrupting studies, some using A22, demonstrate that the bundled MreB filaments participate in establishing the width and stiffness of the cell while exerting an inward force on the cell wall[26-30]. MreB is also known to have other pleitotropic effects on a range of cellular functions and its loss is frequently lethal in model microbial systems[12]. Some Δ*mreB* mutants can be grown for short periods in heavily supplemented media[15]. In A22 treated cells and in transiently viable *ΔmreB* strains the loss of *mreB* function leads to spherical shape and continuous volume increase, lysis and a loss of cell membrane potential [5,20,31-33].

Previous work has demonstrated the viability of *mreB*-defective transposon-generated mutants of otherwise rod-shaped *Pseudomonas fluorescens* SBW25[34]. These mutants produce spherical cells in standard Lysogeny Broth (LB) media. The discovery of a nascent spherical phenotype in the absence of MreB in a rod-like bacterium provides

the opportunity to investigate the consequences of MreB loss and the range of compensatory mutations that might restore fitness.

Here we demonstrate that deletion of *mreB (ΔmreB)* in *P. fluorescens* SBW25 results in viable spherical cells with decreased fitness and highly variable cell size. Evolving this mutant for 1,000 generations in ten independent lineages led to recovery of both WT fitness and cell volume whilst retaining spherical cell shape. Three primary compensatory mutations are studied, two mutations in a PBP (Pencillin Binding Protein) and a separate five-gene deletion. Morphological and single cell time-lapse analysis of strains carrying these mutations demonstrate that these mutations affect lateral cell wall synthesis and septation frequency, reducing sister cell growth asymmetry and proliferation arrest in these cells. Finally, we use comparative genomics of rod–like and spherical cells to infer that PBP loss is a common phenomenon in the evolution of spherical species. Together, our results highlight possible mutational routes by which rod-like cells can adapt their genetic machinery to cope with MreB loss and spherical cell shape.

2 Methods

Bacterial strains and culture conditions

Escherichia coli, *Neisseria lactamica*, and *Staphylococcus aureus* were grown at 37°C, whilst *Lactococcus lactis* cremoris was grown at 30°C, and *P. fluorescens* SBW25 at 28°C. Antibiotics were used at the following concentrations for *E. coli* and/or *P. fluorescens* SBW25: 12 μg ml^{-1} tetracycline; 30 μg ml^{-1} kanamycin; 100 μg ml^{-1} ampicillin. Bacteria were propagated in LB.

Strain construction

The *ΔmreB* strain was constructed using SOE-PCR (splicing by overlapping extension using the polymerase chain reaction), followed by a two-step allelic exchange protocol[1]. Genome sequencing confirmed the absence of suppressor mutations. The same procedure was used to reconstruct the mutations from the evolved lines (PBP1a G1450A, PBP1a A1084C, ΔPFLU4921-4925) into WT-SBW25 and the Δ*mreB* backgrounds. DNA fragments flanking the gene of interest were amplified using two

primer pairs. The internal primers were designed to have overlapping complementary sequences which allowed the resulting fragments to be joined together in a subsequent PCR reaction. The resulting DNA product was TA-cloned into pCR8/GW/TOPO (Invitrogen). This was then subcloned into the pUIC3 vector, which was mobilized via conjugation into SBW25 using pRK2013. Transconjugants were selected on LB plates supplemented with nitrofurantoin, tetracycline and X-gal. Allelic exchange mutants identified as white colonies were obtained from cycloserine enrichment to select against tetracycline resistant cells, and tetracycline sensitive clones were examined for the deletion or mutations using PCR and DNA sequencing.

Evolution Experiment

Ten replicate populations of the Δ*mreB* strain were grown in 5 mL aliquots of LB broth at 28°C with shaking at 180 rpm. Every 24 h, 5 µL was transferred to fresh media. Every 5 days, samples of each population were collected and stored at -80°C in 15% (v/v) glycerol. The number of generations per transfer changed over the course of the experiment but is roughly ten generations per night and ~1,000 generations (100 transfers) were performed.

Competitive fitness assay

Competitive fitness was determined relative to SBW25 marked with GFP. This strain was constructed using the mini-Tn7 transposon system, expressing GFP and a gentamicin resistance marker in the chromosome (mini-Tn7(Gm)PrrnB P1 gfp-a)[2].

Strains were brought to exponential phase in shaken LB at 28°C before beginning the competition. Competing strains were mixed with SBW25-GFP at a 1:1 ratio by adding 150 uL of each strain to 5 mL LB, then grown under the same conditions for 3 hours. Initial ratios were determined by counting 100,000 cells using flow cytometry (BD FACS Diva II). Suitable dilutions of the initial population were plated on LBA plates to determine viable counts. The mixed culture was diluted 1,000-fold in LB, then incubated at 28°C for 24 hours. Final viable counts and ratios were determined as described above. The number of generations over 24 hours of growth were determined using the formula ln(final population/initial population)/ln(2), as previously described[3]. Selection coefficients were calculated using the regression model $s = [\ln(R(t)/R(0))]/[t]$, where R is the ratio of the competing strain to SBW25-

GFP, and t is the number of generations. Control experiments were conducted to determine the fitness cost of the GFP marker in SBW25. For each strain, the competition assay was performed with a minimum of 3 replications. WT SBW25 had a relative fitness of 1.0 when compared to the marked strain, indicating that the GFP insert is neutral, and that the SBW25-GFP strain was a suitable reference strain for this assay.

Microscopy

Cells from liquid culture. Cells were routinely grown in LB, and harvested at log phase (OD_{600} 0.4). Viability assays were conducted using the LIVE/DEAD BacLight Bacterial Viability Kit (Thermo Fisher). Viability was measured as the proportion of live cells in the total population (live/(live +dead)). Nucleoid staining was done using the DAPI nucleic acid stain (Thermo Fisher) following the manufacturer's protocols.

Time-lapse on agarose pads. Strains were inoculated in LB from glycerol stocks and shaken overnight at 28°C. The next day, cultures were diluted 10^2 times in fresh LB and seeded on a gel pad (1% agarose in LB). The preparation was sealed on a glass coverslip with double-sided tape (Gene Frame, Fischer Scientific). A duct was cut through the center of the pad to allow for oxygen diffusion into the gel. Temperature was maintained at 30°C using a custom-made temperature controller[35].(Bacteria were imaged on a custom built microscope using a 100X/NA 1.4 objective lens (Apo-ph3, Olympus) and an Orca-Flash4.0 CMOS camera (Hamamatsu). Image acquisition and microscope control were actuated with a LabView interface (National Instruments). Typically, we monitored 10 different locations; images were taken every 5 min in correlation mode[36]. Segmentation and cell lineage were computed using a MatLab code implemented from Schnitzcell[37]. Bacteria were tracked for 3 generations.

Scanning Electron Microscopy (SEM). Cells were grown in LB, and harvested at log phase. Cells were fixed in modified Karnovsky's fixative then placed between two membrane filters (0.4µm, Isopore, Merck Millipore LTD) in an aluminum clamp. Following three washes of phosphate buffer, the cells were dehydrated in a graded-ethanol series, placed in liquid CO_2, then dried in a critical-point drying chamber. The samples were mounted onto aluminum stubs and sputter coated with gold (BAL-TEC

SCD 005 sputter coater) and viewed in a FEI Quanta 200 scanning electron microscope at an accelerating voltage of 20kV.

Image analysis

Compactness and estimated volume measurements of cells from liquid culture. The main measure of cell shape, compactness or **C**, was computed by the CMEIAS software as: $(\sqrt{4\text{Area}/\pi})/\text{length}$. Estimated volume or $\mathbf{V_e}$ was estimated with different formula, according to cell compactness, for spherical cells that have a compactness ≥ 0.7, $\mathbf{V_e}$ was computed using the general formula for spheroids: $v=4/3\pi(L/2)(W/2)^2$, where L=length and W=width. $\mathbf{V_e}$ of rod-shaped cells, defined as having a compactness value ≤ 0.7, were computed using the combined formulas for cylinders and spheres: $\mathbf{V_e} = (\pi(W/2)^2(L-W))+(4/3\pi(W/2)^3)$.

Cell size, elongation rate, and division axis of cells on agarose pads. Cell size was computed as the area of the mask retrieved after image segmentation. The elongation axis is given by the major axis of the ellipse that fits the mask of the cell. Division axis is the computed by comparing the elongation axis between mother and sister cell, through the following formula: $|\sin\theta|$, where θ is the angle between mother and sister cell. We measured the elongation rate of individual bacteria by fitting the temporal dynamics of cell area with a mono-exponential function. The elongation rate is then given by the rate of the exponential. To obtain the intrinsic cell size and disentangle it from the variability associated to asynchrony in the cell cycle, cell size was measured at cell birth, i.e. right after septation. Cell size was then normalized to the size of the WT strain.

Proliferation probability. For the first and second generations, we computed the proliferation probability as the capability of progressing through the cell cycle and dividing. Bacteria that do not grow or stop elongating before dividing are classified as non-proliferating. For all non-proliferating bacteria, we confirmed that no division occurs for the next 5 hours.

Growth asymmetry. For all sister cell pairs, we computed the asymmetry as the contrast in cell elongation given by: $\left|\frac{r_2-r_1}{r_1+r_2}\right|$, where $r_{1,2}$ are the elongation rate of the

two sisters measured for the second generation. We then computed the population average on the sub-population that proliferates in order to avoid trivial bias due to cell proliferation arrest of one of the two sister cells.

Protein sequence alignment and modeling

Protein sequences were obtained from NCBI BLAST (http://blast.ncbi.nlm.nih.gov) and The Pseudomonas Genome Database[38], and aligned using MEGA7[39]. The sequence alignment was visualised using ESPript 'Easy Sequencing in PostScript' [40].

Protein visualisation was done on Visual Molecular Dynamics (VMD)[41] using the crystal structure of *Acinetobacter baumannii* PBP1a in complex with Aztreonam as the base model, which shares a 73% sequence identity (E value = 0.0) to the PBP1a of *P. fluorescens* SBW25. Sequences were aligned, and locations of the mutations in the evolved lines were mapped in the corresponding regions. The PDB file was downloaded from the RCSB Protein Data Bank (www.rcsb.org) using PDB ID 3UE0.

3 Results

MreB deletion in *P. fluorescens* SBW25 generates viable spherical cells

Δ*mreB* cells to be spherical and display a highly variable cell size and shape compared to the WT strain in phase contrast and SEM (Fig. 1A). The Δ*mreB* strain is viable with approximately 82.5% (±7.9%) live cells compared to WT at 95.2% (±1.2%)(Fig. 1B). Relative fitness in pairwise competition assays demonstrates that the Δ*mreB* strain has a markedly lower relative fitness of 0.78 (±0.02) compared to the WT (Fig. 1C)[42]. The Δ*mreB* strain had a slower generation time of 65 min (WT, 45 min), prolonged lag phase, and lower maximum yield (Supp. Fig. 1).

The *mreB* gene was ectopically expressed from the Tn7 site near the *glmS* region of the Δ*mreB* strain completely restored WT morphology, viability, and relative fitness in the *Δ mreB* cells with slightly delayed growth (longer lag) (Supp. Fig. 2). Therefore the morphological effects seen in Δ*mreB* are considered to be due solely to loss of MreB.

To quantify variability in size and shape we performed a principle components analysis of the shape metrics (CMEIAS software package)[43,44] which motivated a focus on a metric called compactness[4], a measure of the circularity of the cell's outline. A compactness of 1.0 is circular whilst values below 0.7 are more typical of rod-shaped cells. For our purposes, cells with an average compactness of 1.0 to 0.8, before visible septation initiation are considered to be "spherical". The projected cell outlines were used to estimate volume, (**V_e**) (see Material and Methods) and plotted each cell's **V_e** vs compactness for both WT and *ΔmreB* cells (Fig. 1D).

WT cells have a small **V_e** range and a negative correlation between **V_e** and compactness, reflecting the linear elongation and regular cell division of rod-shaped cells. In contrast, the Δ*mreB* strain exhibits large spherical to ovoid cells (, with a wide distribution of **V_e** ranging from 1.12 um^3 to ~90 um^3, averaging 20.65 um^3 (±16.17 um^3). Spherical *ΔmreB* cells initiate septation at a wide range of volumes from 10 um^3 to 90 um^3, indicating that the relationship between cell size and division is lost in *ΔmreB* cells (see lower compactness cells in Fig. 1D).

As cell volume increases, DNA content might also be expected to increase if DNA replication continues irrespective of division frequency. Increased DNA content and spherical cell shape are both predicted to further perturb cell division[45,46]. WT and *ΔmreB* cells were stained with a nucleic acid stain (FITC) to label DNA and subjected to flow cytometry. In both strains DNA content scaled with cell size as measured by Forward Scatter Area (FSC-A). The largest *ΔmreB* cells have many times the DNA content of WT cells, scaling roughly with volume (Fig. 1E, Supp. Fig. 3) indicating that DNA replication continues irrespective of cell size. In addition, WT cells observed by time-lapse, orientation of the division plane is consistent across divisions ($|\sin(\phi)| = 0$). In contrast, in the *ΔmreB* population, septa positioned perpendicularly relative to the last plane at each generation ($|(\sin(\phi)| = 1$) (Fig. 1F, Supp. Fig. 4B). The change from maintaining septation angles to alternating septation suggests that DNA segregation (prior to septation) is perturbed in cells that have lost rod-like shape. This is consistent with similar results obtained from *E. coli* treated with the MreB inhibitor, A22[47].

Experimentally evolving spherical cells

Having established that we have a viable *ΔmreB* in *P. fluorescens* SBW25 an investigation into how this strain adapts to the challenge of MreB loss, was conducted using an experimental evolution approach to select for mutants that restore fitness. After 1,000 generations of evolution (Fig. 2A) the final evolved populations displayed both relative fitness (Fig. 2B) and growth dynamics that were similar to the WT (Supp. Fig. 5). However, the evolved cells remained spherical in shape (Fig. 2D, Supp. Fig. 6). The size, however, as measured by **Ve** had decreased to roughly that of the ancestral cells (Fig. 2D). The **Ve** of the evolved lines does not overlap with the *ΔmreB* population (Fig. 1D), evidence that these evolved cells present a new phenotype and are not a subset of the spherical *ΔmreB* ancestor. These newly evolved spherical cells are most similar in cell shape, particularly at septation, to species like *Lactococcus lactis* cremoris or *Neisseria lactamica* and other spherical bacterial species that still undergo some elongation prior to division, not like *Staphylococcus aureus* (Supp. Fig 11)[48]. The latter experience rapid division as nearly perfect spheres (Supp. Fig.11) [49].

In order to understand the dynamics of the fitness recovery the frozen evolved populations were resuscitated at various time points and competed these pairwise against a GFP labeled WT ancestor (Fig. 2C). The fitness increase during evolution occurred rapidly: after only 50 generations of growth, the evolved lines had an average competitive fitness score of 0.92 (±0.01). This increased to an average fitness of 0.97 (± 0.02) by the end of the experiment.

Identifying mutations compensating for costs arising from deletion of *mreB* .

The rapid fitness increase observed indicates that a small number of mutations arose early and swept through the populations of poorly competing Δ*mreB* cells. In order to identify these mutations, we conducted population sequencing at 500 and 1,000 generations and reference mapped these reads to the *P. fluorescens* SBW25 genome (GCA_000009225.1) to an average read depth of 100 fold. We identified several mutations affecting open reading frames that were found in over 75% of the sequence reads in several evolved lines (detailed, Supp. Table 1). A single gene, *pbp1a* had independent mutations in multiple lines. Representative *pbp1a* mutations from lines 1, 4 were chosen for further study. Line 7 had a five-gene deletion that included the *oprD* homolog which was also chosen for further analysis.

The *pbp1A* gene (PFLU0406) encodes the major Class A penicillin-binding protein responsible for the final steps of peptidoglycan synthesis. PBP1a proteins are key components of peptidoglycan synthesis machinery in the cell wall elongation complexes and are associated with the MreB cytoskeleton in rod-like cells[5].

This PBP1a contains three known domains (Fig. 3A). Structure mapping of the mutations demonstrates that the mutation in Line 1 occurred in a well-conserved region in the transpeptidase (TP) domain, proximal to the active site (Supp. Fig. 7). Similar mutations in *Steptococcus pneumoniae*[50] cause a loss of function in this domain. The mutation in Line 4 took place in the oligonucleotide/oligosaccharide binding (OB) domain[6]. These will be referred to from hereon as the *pbp1a* Line 1 and Line 4 mutations respectively. In order to determine the effects of these mutations on cell shape and growth, these separately reconstructed in the WT and Δ*mreB* backgrounds.

The *ΔmreB pbp1A* mutation strains remained spherical to ovoid, near WT volume and DNA content (Fig. 3D, Supp. Fig. 9). These cells also retained the shorter generation times (48 min), growth dynamics (Supp. Fig. 8) and relative fitness of the evolved line populations (Fig. 3C), suggesting that the *pbp1A* mutations are each sufficient to both restore WT fitness and to recapitulate the major phenotypes of evolved lines 1 and 4.

The function of PBP1A in the ancestral strain and therefore the presence of MreB, is not well studied. The same mutations were therefore reconstructed in the WT background. The WT *pbp1a* mutations also had generation times, growth curves (Supp. Fig. 7) and relative fitness measures similar to WT (Fig. 3C).

The major phenotypic difference in the presence of the *pbp1a* mutations was that both the *Pbp1a TP* and *OB* mutation reconstructions had rod-like cells that are significantly narrower in cell widths (0.89 um ± 0.07, 0.94 um ± 0.05 respectively) compared to WT (1.00 um ± 0.06) ($p = <0.001$). This resulted in smaller cell volumes (Fig. 3E and Supp. Fig. 9). This decrease in cell width as a result of an amino acid change near the transpeptidase domain of an elongasome-component is evidence that this mutation decreases the function of PBP1a, likely by interfering with transpeptidase function

(Fig. 3E in Blue). The similar phenotype conferred by the OB domain indicates that these domains act similarly in contributing to cell width (Fig. 3E in Green). The cell size decrease also corresponded with a slight decrease in DNA content (Supp. Fig. 3). The production of thinner cells, is consistent with previous work on the effects of PBP1a function loss in both *B. subtilis* and in *E. coli* [51-54]. Based on the positions of the respective mutations, and their resulting phenotypes in WT cells, we interpret these results to indicate that either of these *pbp1A* mutations can reduce lateral cell wall synthesis, resulting in smaller cells when MreB is present.

The other major mutation identified in the evolved lines was a five-gene deletion (PFLU4921-4925) in evolved Line 7 (Fig. 3B, Supp. Table 1). The deletion contains three hypothetical proteins, a cold shock protein (PFLU4922, encoding CspC), and an outer membrane porin, PFLU4925 which encodes OprD. The latter is responsible for the influx of basic amino acids and some antibiotics into the bacterial cell[7]. This deletion was constructed and characterised in the Δ*mreB* and WT backgrounds.

The Δ*mreB* five-gene deletion strain had a generation time and growth dynamics similar to WT, with an additional extended lag time (Supp. Fig. 8). The viability and relative fitness were also highly similar to WT (Fig. 3C). The cells were spherical with an averge **Ve** of 5.32 um^3 (±3.18) (Fig. 3D and Supp. Fig. 8). As in the *pbp1A* Line 1 and Line 4 mutations, DNA content was also decreased compared to the *ΔmreB* ancestor (Supp. Fig. 3). In addition, the five-gene deletion produces cell division defects in 25.61% (±6.42%) of these cells, manifesting as septation defects and connected clumps of spherical cells (Fig 3D, Supp. Fig. 9).

In the WT strain, the five-gene deletion produced rod shaped cells with growth characteristics similar to the WT strain (Supp. Fig 8). These cells were however significantly thinner than WT (width = 0.74um ± 0.06, p = <0.001) and had a smaller average **Ve** of 2.47 um^3 (±1.18) (Fig. 3E and Supp. Fig. 8). As in the *ΔmreB* background, a sub-population exhibits a filamenting phenotype occurring in 20% (± 4%) of the population. The five-gene deletion strains were the only ones that showed evidence of dispersed DNA between incomplete septa in DAPI staining (Supp. Fig S10). Intriguingly, clinically isolated *Pseudomonas* with *oprD* deletions have significant changes in the regulation of the MinCD system[55]. In closely related model

systems MinCD, acts to negatively affect septal placement by poles and accumulating as a result of cell shape asymmetry[17,56-58]. The connection between OprD and MinCD in *Pseudomonas* merits further investigation but *oprD* loss may mitigate large cell size and increase fitness in *ΔmreB* by retuning septation frequencies. This would also imply that the viable *ΔmreB* cells lack proper the geometry required to support MinCD oscillations[59], resulting in erratic septation and driving large cell size.

Sister Cell Asymmetry at the Single Cell Level

In order to determine the basis of the fitness cost of the mreB deletion, we, we conducted single cell experiments in the reconstructed mutants and representative evolved clones from lines 1, 4 & 7. Time-lapse microscopy was used to track individual cells through subsequent generations to measure size, elongation rate, division axis and shape for each cell as well as their capacity to produce two daughters[36,60].

All reconstructed strains except the strain that ectopically expresses *mreB* (closed grey square), have a reduced rate of cell wall synthesis relative to the WT (Fig. 4A) but all are higher than the ancestral *ΔmreB* strain. Cell elongation rates are higher in the presence of MreB in the *pbp1A* Line 4 mutant, but not the Line 1 mutant, suggesting that the transpeptidase domain mutation may affect the degree to which MreB stimulates synthesis[61].

In addition, single cell experiments measured that a fraction of cells underwent persistent proliferation arrest on solid media, even after five hours of observation (Fig. 4B). Tracking pairs of dividing cells coming from the same mother revealed that they experience unequal rates of cell wall synthesis, or 'growth asymmetry' (Fig. 4B). A strong correlation is observed between proliferation arrest and growth asymmetry in our reconstructed mutation strains and representative clones. In strains that had higher growth asymmetry, more proliferation arrest was observed (Fig 4D). This increased growth asymmetry might either initiate proliferation arrest or both features may be symptoms of another attribute of these cells such as cell size or defects in DNA segregation driven by cell shape and septum aberrations[46,62].

Accordingly, cells that have lost MreB are able to find a new equilibrium by decreasing elongation synthesis (*pbp1A* mutations) or possibly modulating septation associated synthesis (the *oprD* inclusive deletion). Either serves to increase the relative proportion of synthesis at the septum, and decrease elongasome associated synthesis. The advantage gained through these adjustments in response to MreB loss hint at a previously unrecognized role of MreB in ensuring the equal partitioning of the elongasome components before and after cell division.

Recapitulating spherical shape evolution

These experiments demonstrate that either a decrease in activity in a PBP in the elongasome or a five-gene deletion that includes *oprD* allow a rebound in fitness when *mreB* is lost. It was previously reported that coccoid bacterial species have lower estimated numbers of PBPs based on estimates from a biochemical function assay[63]. We were therefore interested in whether comparative genomics of completely sequenced bacteria bore this pattern out as well. We therefore selected 26 bacterial species pairs in which one member has maintained rod-like shape and the other has become spherical and compared the abundance of the homologues of the genes implicated in our evolution experiment; MreB, PBPs and OprD homologs. OprD homologs were too rare across species to analyze. However, we observed a significant relationship between coccoid lineages that had lost MreB and a decrease in the number of PBP homologs (avg. PBPs in rods = 9.22 ± 5.15; spheres = 3.89 ± 2.65; difference: $p = <0.001$). From this we infer that species that have naturally evolved from rod-like to spherical shape tend to have lost both *mreB* and approximately half of their PBP genes.

Reshaping a rod-like pseudomonad to be a spherical cell

P. fluorescens SBW25 is a rod-like bacterium that can be reshaped into a rapidly growing spherical cell in as little as two mutational steps, the deletion of *mreB* and either a single amino acid changing mutation in *pbp1A* or an *oprD* inclusive deletion. The reason that this strain is tolerant of MreB loss is not currently known but a separate paralog does not exist in this strain.

The loss of MreB from the ancestral SBW25 causes extremely large cells with multiple chromosomes (Fig. 1D,E) with highly irregular septation. In addition, sister

cells elongate perpendicularly to mother cells, across cell divisions (Fig 1E-F), consistent with MreB disruption experiments using i*li* and *P. aeriginosa*[31,64]. Both cell wall synthesis and DNA replication are continuous in these cells (Fig. 1E and Fig. 4A) meaning that large cell size is the result of a reduction in septation frequency, maybe due to the loss of the ordered relationship between septation and DNA segregation in spherical cells[46].

The *ΔmreB* population had high levels of cell wall synthesis asymmetry and while either of the *pbp1A* mutations increased this symmetry, the five-gene deletion did not (Fig. 4D). This increase in symmetry suggests that the distribution of active elongasomes may be disorganised in cells lacking MreB and that this disorganization is reduced when *pbp1A* is mutated[52](Fig 4C). This raises the possibility that symmetry in cell synthesis is maintained in these cells by continued septal cell wall synthesis. While this is consistent with models of other spherically shaped cells in which much of the cell wall synthesis further investigation of cell wall synthesis is required to support or refute this hypothesis[65-67].

Implications for the evolution of spherical cell shape

The wide array of cell shapes and sizes observed in the eubacteria have arisen from an ancestral rod-like cell shape[2,68-70] Coccoid or spherical cells are the product of a degradation of this shape[14,71]. The transition to spherical cell shape has taken place independently many times[8,72-74] and is associated with *mreB* loss, possibly as an early event[48,49].

This study uncovers separate compensatory mutations that allow rapid fitness recovery after MreB loss. If MreB loss is a common early event in coccus evolution then there are likely to be both genetic and environmental contexts that favor this state[2,9,14,71]. One possibility is that the transient increase in cell size observed in Δ*mreB* cells is advantageous in some settings. This hypothesis compels further investigation[16].

4 Conclusions

Cell shape is a fundamental property of cells that defines motility, DNA segregation,

replication, nutrient acquisition, waste elimination and predator evasion[16]. *P. fluorescens* SBW25 is a rod-shaped bacterium that is amenable to MreB deletion. The loss of MreB is a non-lethal but deleterious event that leads to irregular, large-sized spherical cells. Further, separate mutations can restore fitness and volume whilst retaining spherical cell shape and these are likely decrease-of-function mutations in the gene encoding elongasome member PBP1A, or a five-gene deletion that includes *oprD*. These mutations are able to restore symmetry in cell growth between sister cells and decrease cell death. We therefore propose a model of molecular change when MreB is lost, essentially re-storing symmetric cell wall synthesis by relying more heavily on synthesis at the septum. Last, our study implicates a decrease of PBP function, as a general strategy in cells recovering from the loss of MreB and refining spherical cell shape in bacteria.

Acknowledgements

We thank Olin Silander for helpful discussions and for his assistance to PRY with principle components analysis of cell shape, Sebastian Schmeier and Saumya Agrawal for bioinformatic analysis and Tim Cooper for helpful comments on the manuscript. Electron Microscopy was provided by Massey University and was performed by Niki Murray, Manawatu Microscopy and Imaging Centre, Massey University, Palmerston North, NZ.

Figures

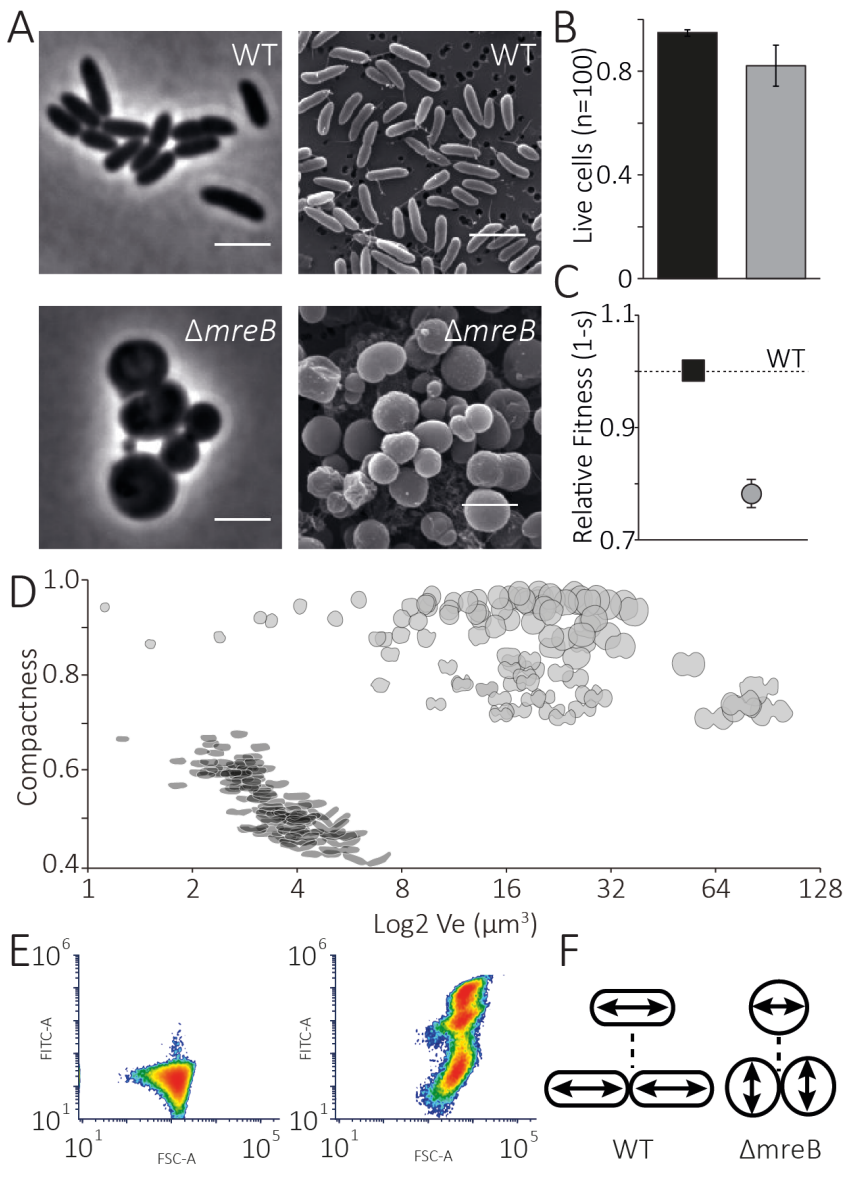

Figure 1. Characterisation of WT and Δ*mreB* strains. Figure shows (A) photomicrographs of WT and Δ*mreB*. Scale bars, 3 µm. B) Proportion of live cells in WT (black bar) and Δ*mreB* (grey bar). Error bars represent standard error (n = 3). C) Fitness of WT GFP and the ancestral Δ*mreB* mutant relative to WT when both are in exponential phase during pairwise competition assays. Error bars as in 1B. D) The relationship between cell shape and estimated volume (V_e) is represented using compactness, a measure of roundness. One hundred representative cells from each WT and Δ*mreB* are shown as cell outlines. E) DNA content (FITC-A) is highly correlated with increased cell sizes (FSC-A) in Δ*mreB* but both are limited in WT cells (n=50,000 events). F) Diagram of WT cells maintaining a single consistent division plane whilst Δ*mreB* cells alternate division planes by 90° from one division to the next.

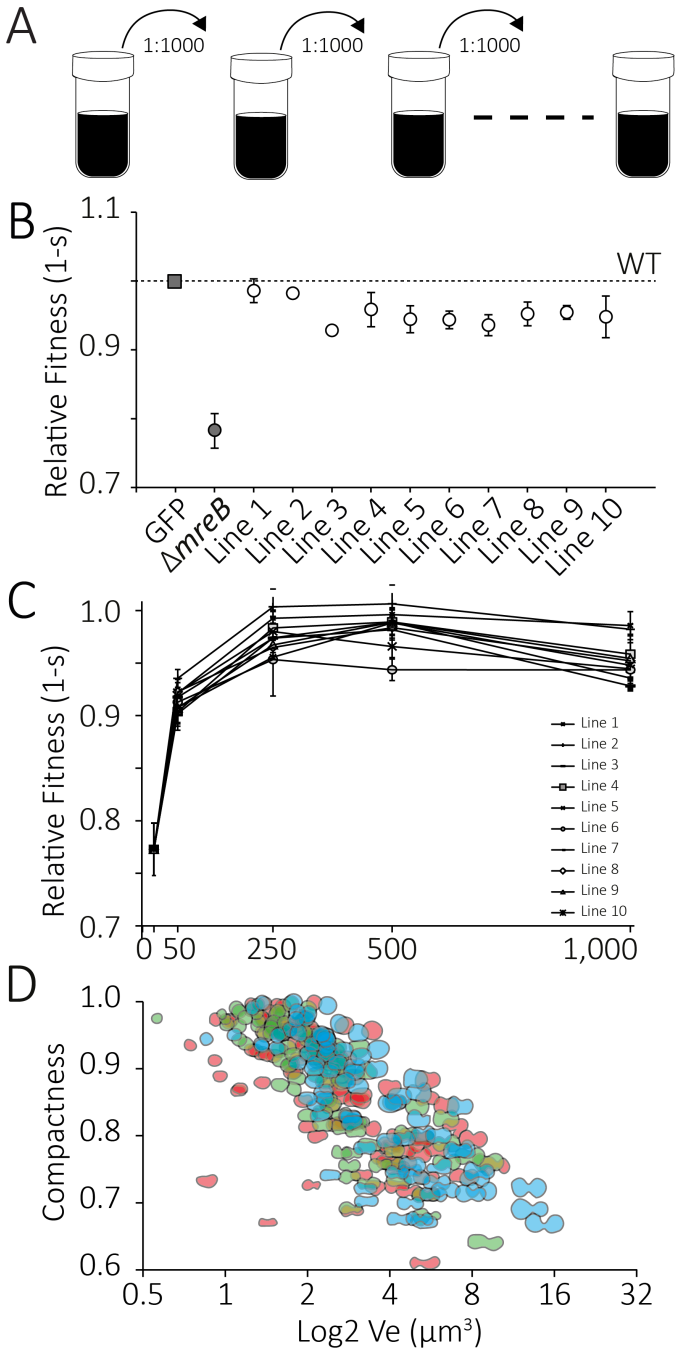

Figure 2. Characterisation of Evolved Lines at 1,000 generations. A) Diagram of evolution experiment protocol. 1:1000 transfer each 24 hours. B) Relative fitness of the Δ*mreB* mutant and evolved lines after ~1,000 generations relative to WT (dashed line) in pairwise competition experiments. Error bars represent standard error (n = 3). C) Relative fitness of the evolved lines during 1,000 generations of growth. Error bars as in B. D) Cell outlines of three representative evolved lines Line 1 in blue, Line 4 in green and line 7 in red. One-hundred randomly chosen cell outlines from each line are depicted.

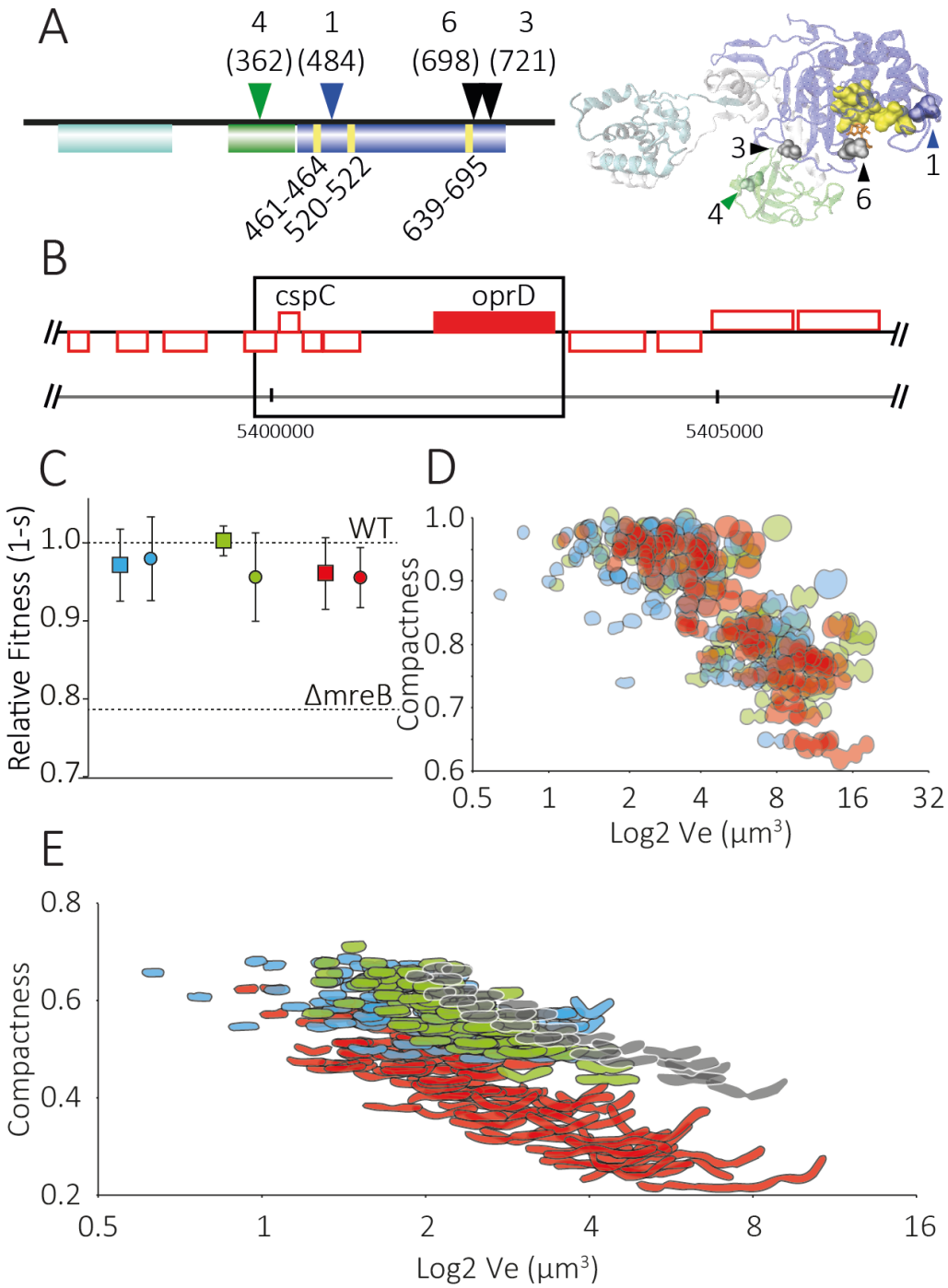

Figure 3. Characterisation of the reconstructed mutations in WT and Δ*mreB* background. A) Domain map and model of PBP1a (PFLU0406) showing the 2 major active sites; the glycosyltransferase (GT) domain (cyan) and the transpeptidase (TP) domain (blue). The oligonucleotide/oligosaccharide binding (OB) domain is shown in green. The active site of the TP domain is also shown (yellow). The mutations identified are indicated above the map. B) Genome map of *oprD* inclusive deletion, (PFLU4921-PFLU4925) and surrounding region. Genes with function calls are noted. C) Relative fitness of the three reconstructed mutants in the Δ*mreB* (circles) and WT

(squares) backgrounds. Line 1 reconstruction, PBP1a D484N is shown in blue, Line 4 PBP1a T362P is shown in green and the OprD containing deletion reconstruction is shown in red. D) Compactness versus estimated volume (Ve) for reconstruction strains in the Δ*mreB* background, colors as in 1C (N=100). E) Compactness versus estimated volume (Ve) of the mutants in the WT background colours and N as in C and D. A subset of WT cells are shown in light grey for comparison.

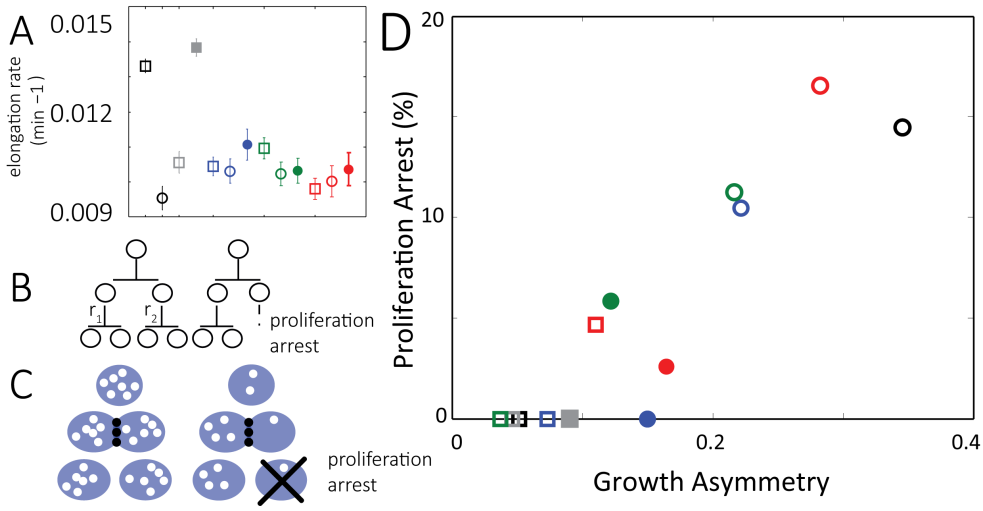

Figure 4. Single cell time-lapse measurements of reconstructed mutations. A) Average population elongation rate for WT, reconstructions and evolved cells. Open square data points represent WT or WT and respective mutations (open grey square = *ΔmreB* with ectopic *mreB*), open circles are Δ*mreB* or *ΔmreB* and respective mutations and closed symbols are evolved cell lines. Colors as in Fig 3; blue is Line 1 or PBP1a D484N, green is Line 4 or PBP1a T362P, red is Line 7 or OprD inclusive deletion. B) Strategy for analyzing single cell measurements during growth on agarose pads including r_1 and r_2. C) Model for relationship between growth asymmetry and proliferation arrest driven by disordered acquisition of cell wall synthesis machinery (white dots). The septum associated PBPs (black circles) at the division plane provide symmetric cell wall synthesis to respective daughter cells. D) Relationship between paired-sister cell proliferation arrest and growth asymmetry in all reconstructions and representative evolved cells (N=100 for each).

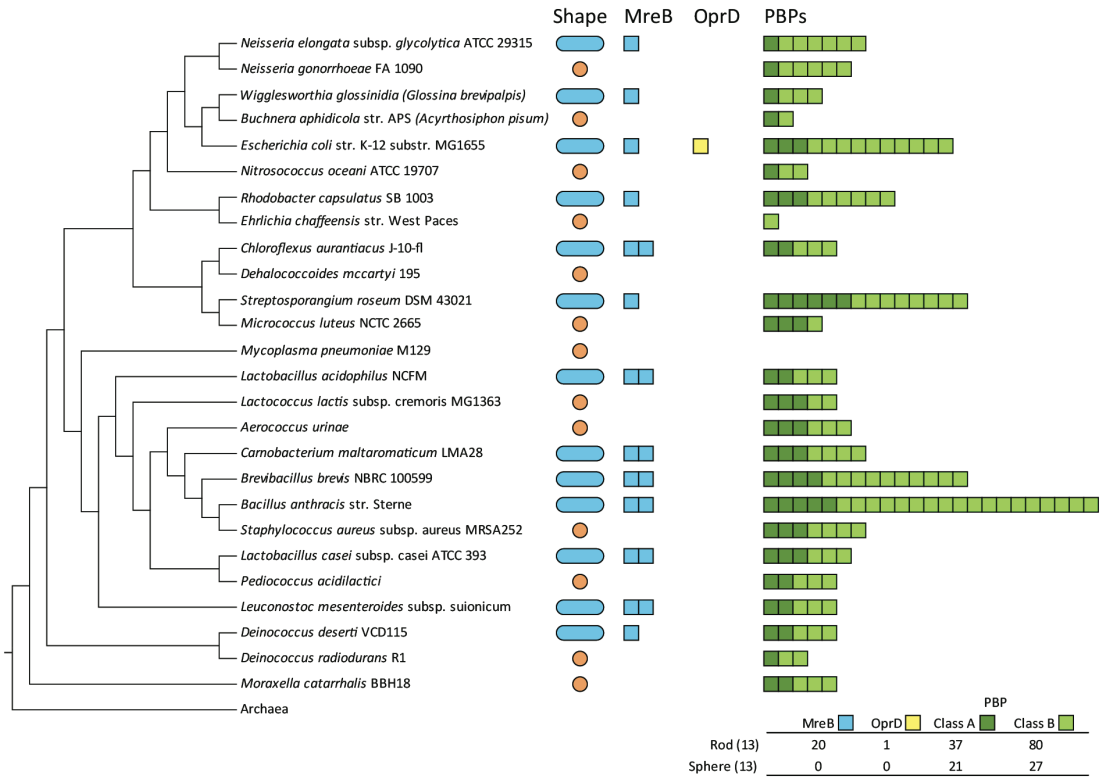

Figure 5. Penicillin-Binding Proteins (PBPs) is observed in extant spherically-shaped cells. A selection of 26 paired rod-shaped and spherical cells were analyzed for their PBP and OprD homologs. The genomes of naturally evolved spherical cells have fewer PBPs than rod-shaped species. OprD homologs were rare.

References:

1. Young, K. D. Bacterial morphology: why have different shapes? *Curr Opin Microbiol* **10,** 596–600 (2007).
2. Young, K. D. Bacterial shape. *Mol Microbiol* **49,** 571–580 (2003).
3. Young, K. D. Bacterial shape: two-dimensional questions and possibilities. *Annu. Rev. Microbiol.* **64,** 223–240 (2010).
4. Huang, K. C., Mukhopadhyay, R., Wen, B., Gitai, Z. & Wingreen, N. S. Cell shape and cell-wall organization in Gram-negative bacteria. *Proc Natl Acad Sci USA* **105,** 19282–19287 (2008).
5. Daniel, R. A. & Errington, J. Control of cell morphogenesis in bacteria: two distinct ways to make a rod-shaped cell. *Cell* **113,** 767–776 (2003).
6. Osborn, M. J. & Rothfield, L. Cell shape determination in Escherichia coli. *Curr Opin Microbiol* **10,** 606–610 (2007).
7. van Teeffelen, S. *et al.* The bacterial actin MreB rotates, and rotation depends on cell-wall assembly. *Proc Natl Acad Sci USA* **108,** 15822–15827 (2011).
8. Siefert, J. L. & Fox, G. E. Phylogenetic mapping of bacterial morphology. *Microbiology (Reading, Engl.)* **144 (Pt 10),** 2803–2808 (1998).
9. Veyrier, F. J. *et al.* Common Cell Shape Evolution of Two Nasopharyngeal Pathogens. *PLoS Genet.* **11,** e1005338 (2015).
10. Margolin, W. Sculpting the bacterial cell. *Curr Biol* **19,** R812–22 (2009).
11. Strahl, H., Bürmann, F. & Hamoen, L. W. The actin homologue MreB organizes the bacterial cell membrane. *Nat Commun* **5,** 3442 (2014).
12. Shaevitz, J. W. & Gitai, Z. The Structure and Function of Bacterial Actin Homologs. *Cold Spring Harbor Perspectives in Biology* **2,** a000364–a000364 (2010).
13. Tamames, J., González-Moreno, M. & Mingorance, J. Bringing gene order into bacterial shape. *TRENDS in ...* (2001).
14. Baidouri, El, F., Venditti, C. & Humphries, S. Independent evolution of shape and motility allows evolutionary flexibility in Firmicutes bacteria. *Nat. ecol. evol.* **1,** 0009–6 (2016).
15. Formstone, A. & Errington, J. A magnesium-dependent mreB null mutant: implications for the role of mreB in Bacillus subtilis. **55,** 1646–1657 (2005).
16. Young, K. D. The selective value of bacterial shape. *Microbiol Mol Biol Rev* **70,** 660–703 (2006).
17. Pichoff, S. & Lutkenhaus, J. Overview of cell shape: cytoskeletons shape bacterial cells. *Curr Opin Microbiol* **10,** 601–605 (2007).
18. Szwedziak, P. & Löwe, J. Do the divisome and elongasome share a common evolutionary past? *Curr Opin Microbiol* **16,** 745–751 (2013).
19. Zhao, H., Patel, V., Helmann, J. D. & Dörr, T. Don't let sleeping dogmas lie: New views of peptidoglycan synthesis and its regulation. *Mol Microbiol* (2017). doi:10.1111/mmi.13853
20. Figge, R. M., Divakaruni, A. V. & Gober, J. W. MreB, the cell shape-determining bacterial actin homologue, co-ordinates cell wall morphogenesis in Caulobacter crescentus. *Mol Microbiol* (2004).
21. Ouzounov, N. *et al.* MreB Orientation Correlates with Cell Diameter in Escherichia coli. *Biophysj* **111,** 1035–1043 (2016).
22. Garner, E. C. *et al.* Coupled, circumferential motions of the cell wall synthesis machinery and MreB filaments in B. subtilis. *Science* **333,** 222–225 (2011).
23. Cava, F., Kuru, E., Brun, Y. V. & de Pedro, M. A. Modes of cell wall growth

differentiation in rod-shaped bacteria. *Curr Opin Microbiol* **16,** 731–737 (2013).

24. Domínguez-Escobar, J. *et al.* Processive movement of MreB-associated cell wall biosynthetic complexes in bacteria. *Science* **333,** 225–228 (2011).
25. Tropini, C. *et al.* Principles of Bacterial Cell-Size Determination Revealed by Cell-Wall Synthesis Perturbations. *CellReports* **9,** 1520–1527 (2014).
26. Ursell, T. S. *et al.* Rod-like bacterial shape is maintained by feedback between cell curvature and cytoskeletal localization. *Proc Natl Acad Sci USA* **111,** E1025–34 (2014).
27. Sun, S. X. & Jiang, H. Physics of bacterial morphogenesis. *Microbiol Mol Biol Rev* **75,** 543–565 (2011).
28. Tuson, H. H. *et al.* Measuring the stiffness of bacterial cells from growth rates in hydrogels of tunable elasticity. *Mol Microbiol* **84,** 874–891 (2012).
29. Garner, E. C., Bernard, R., Wang, W., Zhuang, X. & Rudner, D. Z. Coupled, circumferential motions of the cell wall synthesis machinery and MreB filaments in B. subtilis. *Science* (2011).
30. Hussain, S. *et al.* MreB Filaments Create Rod Shape By Aligning Along Principal Membrane Curvature. *bioRxiv* 1–94 (2017). doi:10.1101/197475
31. Robertson, G. T. *et al.* A Novel Indole Compound That Inhibits Pseudomonas aeruginosa Growth by Targeting MreB Is a Substrate for MexAB-OprM. *Journal of Bacteriology* **189,** 6870–6881 (2007).
32. Kruse, T., Bork-Jensen, J. & Gerdes, K. The morphogenetic MreBCD proteins of Escherichia coli form an essential membrane-bound complex. *Mol Microbiol* **55,** 78–89 (2005).
33. Bendezú, F. O. & de Boer, P. A. J. Conditional lethality, division defects, membrane involution, and endocytosis in mre and mrd shape mutants of Escherichia coli. *Journal of Bacteriology* **190,** 1792–1811 (2008).
34. McDonald, M. J., Gehrig, S. M., Meintjes, P. L., Zhang, X.-X. & Rainey, P. B. Adaptive divergence in experimental populations of Pseudomonas fluorescens. IV. Genetic constraints guide evolutionary trajectories in a parallel adaptive radiation. *Genetics* **183,** 1041–1053 (2009).
35. Julou, T., Desprat, N., Bensimon, D. & Croquette, V. Monitoring microbial population dynamics at low densities. *Rev Sci Instrum* **83,** 074301 (2012).
36. Julou, T. *et al.* Cell-cell contacts confine public goods diffusion inside Pseudomonas aeruginosa clonal microcolonies. *Proc Natl Acad Sci USA* **110,** 12577–12582 (2013).
37. Locke, J. C. W. & Elowitz, M. B. Using movies to analyse gene circuit dynamics in single cells. *Nature Publishing Group* **7,** 383–392 (2009).
38. Winsor, G. L. *et al.* Enhanced annotations and features for comparing thousands of Pseudomonas genomes in the Pseudomonas genome database. *Nucleic Acids Res* **44,** D646–53 (2016).
39. Kumar, S., Stecher, G. & Tamura, K. MEGA7: Molecular Evolutionary Genetics Analysis Version 7.0 for Bigger Datasets. *Mol Biol Evol* **33,** 1870–1874 (2016).
40. Robert, X. & Gouet, P. Deciphering key features in protein structures with the new ENDscript server. *Nucleic Acids Res* **42,** W320–4 (2014).
41. Humphrey, W., Dalke, A. & Schulten, K. VMD: visual molecular dynamics. *J Mol Graph* **14,** 33–8– 27–8 (1996).
42. Lind, P. A., Farr, A. D. & Rainey, P. B. Experimental evolution reveals hidden diversity in evolutionary pathways. *Elife* (2015). doi:10.7554/eLife.07074.001

43. Liu, J., Dazzo, F. B., Glagoleva, O., Yu, B. & Jain, A. K. CMEIAS: A Computer-Aided System for the Image Analysis of Bacterial Morphotypes in Microbial Communities. **41,** 173–194 (2001).
44. Folland, I., Trione, D. & Dazzo, F. Accuracy of Biovolume Formulas for CMEIAS Computer-Assisted Microscopy and Body Size Analysis of Morphologically Diverse Microbial Populations and Communities. *Microb. Ecol.* 1–15 (2014). doi:10.1007/s00248-014-0410-9
45. Jun, S. & Mulder, B. Entropy-driven spatial organization of highly confined polymers: lessons for the bacterial chromosome. *Proc Natl Acad Sci USA* **103,** 12388–12393 (2006).
46. Jun, S. & Wright, A. Entropy as the driver of chromosome segregation. *Nat Rev Micro* (2010). doi:10.1038/nrmicro2391
47. Begg, K. J. & Donachie, W. D. Division planes alternate in spherical cells of Escherichia coli. *Journal of Bacteriology* **180,** 2564–2567 (1998).
48. Zapun, A., Vernet, T. & Pinho, M. G. The different shapes of cocci. *FEMS Microbiology Reviews* **32,** 345–360 (2008).
49. Pinho, M. G., Kjos, M. & Veening, J.-W. How to get (a)round: mechanisms controlling growth and division of coccoid bacteria. *Nature Publishing Group* **11,** 601–614 (2013).
50. Job, V., Carapito, R., Vernet, T., Dessen, A. & Zapun, A. Common alterations in PBP1a from resistant Streptococcus pneumoniae decrease its reactivity toward beta-lactams: structural insights. *J Biol Chem* **283,** 4886–4894 (2008).
51. Murray, T., Popham, D. L. & Setlow, P. Bacillus subtilis cells lacking penicillin-binding protein 1 require increased levels of divalent cations for growth. *Journal of Bacteriology* **180,** 4555–4563 (1998).
52. Kawai, Y., Daniel, R. A. & Errington, J. Regulation of cell wall morphogenesis in Bacillus subtilis by recruitment of PBP1 to the MreB helix. *Mol Microbiol* **71,** 1131–1144 (2009).
53. Banzhaf, M. *et al.* Cooperativity of peptidoglycan synthases active in bacterial cell elongation. *Mol Microbiol* **85,** 179–194 (2012).
54. Claessen, D. *et al.* Control of the cell elongation-division cycle by shuttling of PBP1 protein in Bacillus subtilis. *Mol Microbiol* **68,** 1029–1046 (2008).
55. Skurnik, D., Roux, D. & Cattoir, V. Enhanced in vivo fitness of carbapenem-resistant oprD mutants of Pseudomonas aeruginosa revealed through high-throughput sequencing. in (2013). doi:10.1073/pnas.1221552110/-/DCSupplemental
56. Shih, Y. L., Kawagishi, I. & Rothfield, L. The MreB and Min cytoskeletal-like systems play independent roles in prokaryotic polar differentiation. **58,** 917–928 (2005).
57. Chien, A.-C., Hill, N. S. & Levin, P. A. Cell Size Control in Bacteria. **22,** R340–R349 (2012).
58. Corbin, B. D., Yu, X.-C. & Margolin, W. Exploring intracellular space: function of the Min system in round-shaped Escherichia coli. *EMBO J* **21,** 1998–2008 (2002).
59. Halatek, J. & Frey, E. Highly canalized MinD transfer and MinE sequestration explain the origin of robust MinCDE-protein dynamics. *CellReports* **1,** 741–752 (2012).
60. Desprat, N., Richert, A., Simeon, J. & Asnacios, A. Creep function of a single living cell. *Biophysj* **88,** 2224–2233 (2005).
61. Typas, A., Banzhaf, M., Gross, C. A. & Vollmer, W. From the regulation of

peptidoglycan synthesis to bacterial growth and morphology. *Nature Publishing Group* **10,** 123–136 (2011).

62. Bigot, S., Sivanathan, V., Possoz, C., Barre, F.-X. & Cornet, F. FtsK, a literate chromosome segregation machine. **64,** 1434–1441 (2007).
63. Lleo, M. M., Canepari, P. & Satta, G. Bacterial cell shape regulation: testing of additional predictions unique to the two-competing-sites model for peptidoglycan assembly and isolation of conditional rod-shaped mutants from some wild-type cocci. *Journal of Bacteriology* **172,** 3758–3771 (1990).
64. Bendezú, F. O. & de Boer, P. A. J. Conditional lethality, division defects, membrane involution, and endocytosis in mre and mrd shape mutants of Escherichia coli. *Journal of Bacteriology* **190,** 1792–1811 (2008).
65. Pérez-Núñez, D. *et al.* A new morphogenesis pathway in bacteria: unbalanced activity of cell wall synthesis machineries leads to coccus-to-rod transition and filamentation in ovococci. *Mol Microbiol* **79,** 759–771 (2011).
66. Lleo, M. M., Canepari, P. & Satta, G. Bacterial cell shape regulation: testing of additional predictions unique to the two-competing-sites model for peptidoglycan assembly and isolation of conditional rod-shaped mutants from some wild-type cocci. *Journal of Bacteriology* **172,** 3758–3771 (1990).
67. Monteiro, J. A. O. M. *et al.* Cell shape dynamics during the staphylococcal cell cycle. *Nat Commun* **6,** 1–12 (2015).
68. Young, K. D. Bacterial Shape: Two-Dimensional Questions and Possibilities. **64,** 223–240 (2010).
69. Koch, A. L. Were Gram-positive rods the first bacteria? *Trends Microbiol* **11,** 166–170 (2003).
70. Errington, J. L-form bacteria, cell walls and the origins of life. *Open Biology* **3,** 120143–120143 (2013).
71. Siefert, J. L. & Fox, G. E. Phylogenetic mapping of bacterial morphology. *Microbiology (Reading, Engl.)* **144 (Pt 10),** 2803–2808 (1998).
72. Stackebrandt, E. & Woese, C. R. A phylogenetic dissection of the family micrococcaceae. *Curr. Microbiol.* **2,** 317–322 (1979).
73. Tamames, J., González-Moreno, M., Mingorance, J., Valencia, A. & Vicente, M. Bringing gene order into bacterial shape. *Trends Genet* **17,** 124–126 (2001).
74. Baidouri, El, F., Venditti, C. & Humphries, S. Independent evolution of shape and motility allows evolutionary flexibility in Firmicutes bacteria. *Nat. ecol. evol.* **1,** 0009–6 (2016).